

DESIGN AND OPTIMIZATION OF WIDE-ANGLE DIFFRACTIVE OPTICAL ELEMENTS

THIS IS A TEMPORARY TITLE PAGE
It will be replaced for the final print by a version
provided by the registrar's office.

Thèse n. 1234 2020
présentée le 16 septembre 2020
à la Faculté des sciences de base
laboratoire SuperScience
programme doctoral en SuperScience
École polytechnique fédérale de Lausanne
pour l'obtention du grade de Docteur ès Sciences
par

Dong Cheon KIM

acceptée sur proposition du jury :

Prof Name Surname, président du jury
Prof Name Surname, directeur de thèse
Prof Name Surname, rapporteur
Prof Name Surname, rapporteur
Prof Name Surname, rapporteur

Lausanne, EPFL, 2020





Abstract

This thesis aims to extend the range of Diffractive Optical Element (DOE) applications by developing models, algorithms and optimization techniques for DOEs with diffraction angles over 45° , which is far beyond the limits of scalar paraxial diffraction model.

Contents

Abstract	i
List of Symbols	v
Introduction	1
1 Methods of Diffractive Optical Elements Design	3
1.1 Diffraction models	3
1.1.1 Rigorous electromagnetic theory	4
1.1.2 Scalar diffraction theory	5
1.2 Inverse design methods	5
1.2.1 Gradient-based optimization	6
1.2.2 Step-transition perturbation approach	7
1.2.3 Adjoint method	9
2 Optimization based on Perturbation Approach	11
2.1 Process of optimization	11
2.1.1 Figure of Merit	11
2.1.2 Design parameters	11
2.1.3 Initial design	11
2.1.4 Gradient calculation	11
2.2 One-dimensional diffractive optical elements	12
2.2.1 Reconstruction results	12
2.2.2 Experimental results	13
2.3 Limits of optimization by STPA	13
3 Optimization based on Adjoint-State Method	15
3.1 Process of optimization	15
3.1.1 Binarization	15
3.1.2 Critical demension	16
3.2 One-dimensional diffractive optical elements	16
3.2.1 Reconstruction results	16
3.2.2 Comparison with results by STPA	16
3.3 Two-dimensional diffractive optical elements	16

Contents

3.3.1	Reconstruction results	17
3.3.2	Experimental results	18
4	Experimental Verification and Fabrication Errors	21
4.1	Fabrication process	21
4.1.1	Laser direct writing	21
4.1.2	E-beam lithography	21
4.2	Measurement set-up	21
4.2.1	Fresnel loss	21
4.3	Fabrication errors	21
4.3.1	Edge shift	21
4.3.2	Effects of fabrication errors	21
4.3.3	Robust design	21
5	Conclusion and Perspectives	23
A	An appendix	25
	Bibliography	27
	Curriculum Vitae	29



List of Symbols

CD	critical dimension
DOE	diffractive optical element

Introduction

Diffractive optical elements (DOEs) are used in a wide variety of applications.

Motivation

This thesis aims to design, build and optimize DOEs operating in more complex diffraction regimes than scalar paraxial theory, with a view to obtaining higher performance components (improved diffraction efficiency, larger diffraction angles, etc) and in this way address applications which are for the moment inaccessible.

Outline of thesis

With respect to the content of this PhD research, the thesis will be organized as follows.

1 Methods of Diffractive Optical Elements Design

In this chapter, we will introduce the theoretical background of the various different ways of modeling the diffraction process. These models constitute the key part of the algorithms developed to simulate and optimize Diffractive Optical Elements (DOEs). The validity regions and computational constraints will be analysed in details to identify the practical limits of different diffraction models.

1.1 Diffraction models

Diffractive optical elements are microstructures employed in the modulation of the properties of light. Since the structures often comprise wavelength-scale features, accurate analysis of the problem requires that light be treated as an electromagnetic wave. Thus, we begin by introducing Maxwell's equations, which describe the properties of an electromagnetic field facilitating accurate calculation of most diffractive phenomena. Several approximate methods are also briefly described in the end of this part.

DOEs consist of surface reliefs with dimensions in micrometer ranges. The micro-structure permits the generation of a spatial distribution of light beams by modulating and transforming the amplitude and/or phase of the light propagated through them. For the purpose of the simplicity, we consider only y invariant wave propagation, i.e., the waves are assumed to propagate along the xz plane.

A diffraction grating is a periodic structure that produces an array of regularly spaced beams by modulating the amplitude or the phase of the incident field. The figure illustrates the propagation through a binary grating with period g and thickness d . The field illuminates the grating at an incident angle θ . The grating generates a set of transmitted and reflected diffraction orders. n_1 and n_2 are the refractive indices of air and a dielectric region, respectively. The fields before and after the grating region can be represented as sums of reflected and transmitted wave components.

$$\begin{aligned}
 U(x, z) &= \sum_{m=-\infty}^{\infty} R_m \exp[i k_{xm} x - i k_z z] & \text{if } z \leq 0 \\
 U(x, z) &= \sum_{m=-\infty}^{\infty} T_m \exp[i k_{xm} x - i k_z (z - d)] & \text{if } z \geq d
 \end{aligned} \tag{1.1}$$

where the complex amplitudes of the diffraction orders R_m and T_m are

$$\begin{aligned}
 R_m &= \frac{1}{g} \int_0^g U(x, 0) \exp(-i k_{xm} x) dx \\
 T_m &= \frac{1}{g} \int_0^g U(x, d) \exp(-i k_{xm} x) dx
 \end{aligned} \tag{1.2}$$

the wave vector component k_x can only certain discrete values $k_{xm} = k_{x0} + 2\pi m/g$, where m is an diffraction order. The propagation angle θ_m of the m th diffraction order can be obtained from the grating equation

$$n_2 \sin \theta_m = n_1 \sin \theta_i + m \lambda / g \tag{1.3}$$

while for the reflected diffraction orders one replaces n_2 by n_1 in eq. (1.3) The diffraction efficiency η_m is defined as the amount of light intensity that ends up into transmitted diffraction order.

1.1.1 Rigorous electromagnetic theory

Various rigorous techniques can be applied to calculate the diffraction efficiency of such a grating by solving Maxwell's equations analytically. In the modulated region of the grating for RCWA shown in Figure with the profile divided into z -invariant slices in which the refractive index distribution in the x -direction. The principle of the method is to present the refractive index profile and the field inside the grating region as Fourier series. The eigenvalue equation is solved for the waveguide modes in each slice. Finally, the resulting field expansion is matched at the interfaces of the slices with the boundary conditions under considering polarization, i.e., TE polarization and TM polarization. The number of eigenmodes taken into count needs to be chosen to sufficiently large. The parameter is defined as M , which is referred to as Fourier orders $-M : M$. The accuracy of the simulation depends on this parameter. The convergence of the calculations has to be checked by simulating the diffraction efficiency as a function of the number of Fourier orders. If the efficiency reaches a stable value, the number of Fourier orders is high enough to ensure reliable results. Generally, TM polarization converges much slower than TE polarization.

1.1.2 Scalar diffraction theory

A simple approximate approach to determine the complex amplitudes and the diffraction efficiencies of the diffraction orders is to use the thin element approximation (TEA) [1]. This method is often called scalar approximation or scalar theory in diffractive optics. When the grating is thin (the order of the wavelength) and with the minimum features of the structure, so call critical dimension, which is at least 10λ , the optical path calculation yields sufficient accuracy for field distribution after the gratings. In TEA the effect of gratings can be described by multiplying the incident field $U_0(x, 0)$ with a complex-amplitude transmission function $t(x)$. we can express the transmitted field as

$$U_t(x, d) = t(x)U_0(x, 0) \quad (1.4)$$

where d is the depth of the grating. the transmission function is defined by calculating the optical path through the structure

$$t(x) = \exp \left[ik \int_0^d n(x, z) dz \right] \quad (1.5)$$

where $n(x, z)$ is the complex refractive index distribution of the grating. Also in TEA, the complex amplitudes T_m of the transmitted diffraction orders are obtained using Fraunhofer approximation

1.2 Inverse design methods

The design methods for DOEs have been refined to such a degree that it has become possible to manipulate light in the almost arbitrary way. The goal of the grating design procedure is to find a structure that generates the required signal with the best possible diffraction efficiency.

The iterative Fourier transform algorithm (IFTA) is one of the most popular methods for designing the DOEs in the paraxial domain. IFTA has proved a powerful design approach that can easily be adapted for a variety of different design problems.

Optimization, so call inverse design, of the diffraction structure, involves modifying an initial design to maximize or minimize a figure of merit which describes the grating's performance. Optimization of various types of parameters is a classical problem in diffractive optics. There are several widely used parametric optimization methods: Downhill Simplex method of Nelder-Mead, Powell's method, and simulated annealing. Especially, simulated annealing is the one of global optimization algorithms can be utilized in order to avoid local minima of the merit function.

A usual task in the design of DOEs is to find a suitable profile shape, for example, by an optimization process. Figure shows an example of a grating profile characterized by by depth d , grating period g and transition points x_k . Normally, some parameters are selected as free

optimization parameters, while others are fixed during the calculations.

The use of optimization tools based on the combination of rigorous analysis and parametric optimization is often computationally heavy. we can use this method for the one-dimensional gratings with small gratings period, e.g., $g \leq 10\lambda$. Therefore, the optics and photonics community has investigated efficient methods for optimization techniques as demonstrated by the numerous optimizations of efficient splitters, couplers, etc

1.2.1 Gradient-based optimization

To obtain quick and stable convergence with high diffraction efficiency and low uniformity error, we use conjugate gradient methods. The coordinates of transition points \vec{x}_n and x_{n+1} before and after the n th iteration are related by

$$x_{n+1}^{\rightarrow} = \vec{x}_n + \vec{h}(\vec{x}_n) t \quad (1.6)$$

with

$$\vec{h}(\vec{x}_n) = -\vec{g}(\vec{x}_n) + \gamma_n \vec{h}(x_{n-1}^{\rightarrow}) \quad (1.7)$$

where $\vec{g}(\vec{x}) = (g_1(\vec{x}), \dots, g_{2K}(\vec{x})) = (\frac{\partial \varepsilon(\vec{x})}{\partial x_1}, \dots, \frac{\partial \varepsilon(\vec{x})}{\partial x_{2K}})$ is the gradient of the Figure of merit, t is the step of the gradient method, and

$$\gamma_n = -\frac{\{\vec{g}(\vec{x}_n) - \vec{g}(x_{n-1}^{\rightarrow})\} \cdot \vec{g}(\vec{x}_n)}{|\vec{g}(x_{n-1}^{\rightarrow})|^2} \quad (1.8)$$

To define the step t of the gradient method, we consider the merit function along the conjugate direction as a function of t

$$\varepsilon \left[\vec{x}_n + \vec{h}(\vec{x}_n) t \right] = \varepsilon_1(t) \quad (1.9)$$

The optimum step size t can be determined by forming a second-order Taylor series expansion of $\varepsilon_1(t)$ about the point $t = 0$

$$\varepsilon_1(t) = \varepsilon_1(0) + \varepsilon_1'(0)t + \frac{\varepsilon_1''(0)t^2}{2} \quad (1.10)$$

The second-order expansion of $\varepsilon_1(t)$ takes a minimum at the t value given by

$$t = -\frac{\varepsilon_1'(0)}{\varepsilon_1''(0)} \quad (1.11)$$

The derivatives $\varepsilon_1'(0)$ and $\varepsilon_1''(0)$ can be obtained from the analytical formula of diffraction efficiencies η_m given by equation. In this method, the thing is that we can describe the gradient of figure of merit in equation, i.e. $\vec{g}(\vec{x})$ with respect to transition points $\vec{x} = (x_1, \dots, x_{2K})$.

$$g_i(\vec{x}) = \sum_{m=-N}^N 2 [\eta_m(\vec{x}) - \hat{\eta}] \left(\frac{\partial |T_m|^2}{\partial \vec{x}} + \frac{\partial |D_m|^2}{\partial \vec{x}} + \frac{\partial T_m^* D_m}{\partial \vec{x}} + \frac{\partial T_m D_m^*}{\partial \vec{x}} \right) \quad (1.12)$$

where $\eta_m(\vec{x})$ is calculated by equation and the each derivatives of Fourier coefficient can be expressed by analytical equation. the analytical solution of gradient of diffraction efficiency was described in Appendix 1.

1.2.2 Step-transition perturbation approach

The sharp material discontinuities at the edges of the aperture mainly contribute to make the diffraction pattern. The perturbations are observed in the field distribution directly after sharp vertical transitions of binary gratings. The TEA calculation, however, yields the constant amplitude and phase. This omission of perturbations in TEA makes computing inaccurate within wavelength-scale structures, the so-called non-paraxial domain. Thus, we can accurately calculate the diffraction efficiency using the model which combines the TEA with field disturbances caused by sharp transitions in the surface profile calculated by RCWA. We define the field perturbation after the k :th sharp transition located at the point x_k in the surface profile as

$$p_k(x) = \begin{cases} U_k^R(x) - U_k^T(x) & \text{if } |x| < \Delta_T \\ 0 & \text{elsewhere} \end{cases} \quad (1.13)$$

where $U_k^R(x)$ and $U_k^T(x)$ are field calculated by RCWA and TEA, respectively and Δ_T is the truncation parameter that is chosen 10λ in the calculations. In Fig. ??, the amplitude and phase of the field distribution directly after an isolated step transition determined by TEA and RCWA is presented. The field perturbations of binary gratings consist of only two kinds of oscillation corresponding to left-side and right-side transition point in a ridge. Therefore, the constructed field behind binary grating with many transition points is described by the x-axis shifts of the two field perturbations p_1 and p_2 in the following expression.

$$\begin{aligned} U(x) &= U^T(x) + \sum_{k=1}^{2K} p_k(x) \\ &= U^T(x) + \sum_{k=1}^K p_1(x - x_{2k-1}) + \sum_{k=1}^K p_2(x - x_{2k}) \end{aligned} \quad (1.14)$$

where $2K$ is the total number of the transitions. Due to the periodicity of the element, the diffraction amplitude of m :th order in far field is given by m :th Fourier coefficient of $U(x)$ as

$$\begin{aligned} A_m &= \frac{1}{g} \int_0^g U(x) \exp(-i2\pi mx/g) dx \\ &= T_m + D_m \end{aligned} \quad (1.15)$$

where g is the grating period and T_m and D_m is the Fourier coefficient of the field calculated by TEA and a field perturbation contribution, respectively.

$$\begin{aligned} T_m &= \frac{1}{g} \int_0^g U^T(x) \exp(-i2\pi mx/g) dx \\ D_m &= P_m \sum_{k=1}^K \exp(-i2\pi mx_{2k-1}/g) + P_{-m} \sum_{k=1}^K \exp(-i2\pi mx_{2k}/g) \end{aligned} \quad (1.16)$$

where the Fourier coefficient P_m of field perturbation $p_1(x)$ is expressed as

$$P_m = \frac{1}{g} \int_0^g p_1(x) \exp(-i2\pi mx/g) dx \quad (1.17)$$

The Fourier coefficient of $p_2(x)$ is P_{-m} in Eq. 1.16 because the $p_2(x)$ is an even function of $p_1(x)$. We found D_m in Eq. 1.16 using the Fourier shifting theorem

STPA is an efficient computation method compared with the calculation by RCWA. Once we get the Fourier coefficient of the field perturbations P_m and P_{-m} , they are stored in a memory, and no further RCWA calculation and Fourier transform calculation are necessary. Also, P_m contains no explicit dependence on transition point x_k . This point is highly useful when calculating the gradient of diffraction efficiencies with respect to transition points to optimize the structures. Finally, for one-dimensional binary gratings, the Fourier coefficient A_m can be expressed as an analytic solution as a function of transition points x_k .

Once the gradient $\nabla_{\mathbf{x}}F$ is known, various algorithms are available to optimize the profile.

A gradient search; an optimization consisting of a gradient minimization of a figure of merit $F(\mathbf{x})$ searching for the best profile, is the iterative correction of the set of transition points \mathbf{x} . We can calculate the gradient of diffraction properties with respect to transition points using STPA because the diffraction efficiencies η_m calculated by STPA can be expressed as a function of transition point x_k .

Generally, the main problem associated with gradient-based tools is the choice of initial inputs to obtain a stable convergence. To obtain quick and stable convergence, we used the initial profile designed by IFTA. While the designed one using IFTA is no more optimal in the non-paraxial domain, it is expected to have strong local optimum around it.

In this study, we use conjugate gradient methods. The coordinates of transition points \mathbf{x}_n and \mathbf{x}_{n+1} before and after the n th iteration are related by

$$\mathbf{x}_{n+1} = \mathbf{x}_n + \alpha_n \mathbf{g}_n \quad (1.18)$$

where \mathbf{g}_n is the search direction, i.e. gradient based on STPA for iteration n , and α_n is the accepted step size from the line search. It provides a way to search for a better point along a line in high-dimensional space, which often involves multiple iterations that do not count towards the major iterations. The gradient is calculated using STPA to get the analytical derivatives.

Meanwhile, the diffraction efficiency which is used for line search procedures is evaluated using RCWA during the optimization process.

1.2.3 Adjoint method

We show in this section the mathematical framework of adjoint method using in our wide-angle DOEs optimizations. we can calculate electromagnetic field in isotropic medium from given illumination by using time-independant Maxwell's equation:

$$\begin{aligned}\nabla \times \mathbf{E} &= i k_0 \mu(\mathbf{r}) \mathbf{H} \\ \nabla \times \mathbf{H} &= -i k_0 \epsilon(\mathbf{r}) \mathbf{E}\end{aligned}\tag{1.19}$$

where $\mu(\mathbf{r})$ and $\epsilon(\mathbf{r})$ is permeability and permittivity at location \mathbf{r} , respectively. For small perturbation in permeability and permittivity, the variation of electromagnetic field is the solution of following equations:

$$\begin{aligned}\nabla \times (\mathbf{E} + \Delta \mathbf{E}) &= i k_0 [\mu(\mathbf{r}) + \Delta \mu(\mathbf{r})] (\mathbf{H} + \Delta \mathbf{H}) \\ \nabla \times (\mathbf{H} + \Delta \mathbf{H}) &= -i k_0 [\epsilon(\mathbf{r}) + \Delta \epsilon(\mathbf{r})] (\mathbf{E} + \Delta \mathbf{E}).\end{aligned}\tag{1.20}$$

We can simplify Eq.1.20 by neglecting the $O(\Delta^2)$ terms so that equation becomes:

$$\begin{aligned}\nabla \times \Delta \mathbf{E} &= i k_0 [\mu(\mathbf{r}) \Delta \mathbf{H} + \Delta \mu(\mathbf{r}) \mathbf{H}] \\ \nabla \times \Delta \mathbf{H} &= -i k_0 [\epsilon(\mathbf{r}) \Delta \mathbf{E} + \Delta \epsilon(\mathbf{r}) \mathbf{E}]\end{aligned}\tag{1.21}$$

which is a valid approximation if the change in the electromagnetic field from $\Delta \mu$ and $\Delta \epsilon$ is sufficiently small. The addition of this tiny perturbation $\Delta \mu$ and $\Delta \epsilon$ at location \mathbf{r} can be treated as the dipole with polarization density \mathbf{P} and a magnetization density \mathbf{M} given by:

$$\mathbf{P}(\mathbf{r}) = \Delta \epsilon(\mathbf{r}) \mathbf{E}(\mathbf{r}) \quad \mathbf{M}(\mathbf{r}) = \Delta \mu(\mathbf{r}) \mathbf{H}(\mathbf{r})\tag{1.22}$$

By introducing Green's tensors, this dipole produces scattered fields to location \mathbf{r}' , which are described by:

$$\begin{aligned}\Delta \mathbf{E}(\mathbf{r}') &= \hat{\mathbf{G}}_{EP}(\mathbf{r}', \mathbf{r}) \mathbf{P}(\mathbf{r}) + \hat{\mathbf{G}}_{EM}(\mathbf{r}', \mathbf{r}) \mathbf{M}(\mathbf{r}) \\ \Delta \mathbf{H}(\mathbf{r}') &= \hat{\mathbf{G}}_{HP}(\mathbf{r}', \mathbf{r}) \mathbf{P}(\mathbf{r}) + \hat{\mathbf{G}}_{HM}(\mathbf{r}', \mathbf{r}) \mathbf{M}(\mathbf{r})\end{aligned}\tag{1.23}$$

where $\mathbf{M}(\mathbf{r})$ terms can be omitted because $\Delta \mu(\mathbf{r}) = 0$ in our material. In addition, the Green's tensors in a reciprocal medium can be expressed by:

$$\begin{aligned}\hat{\mathbf{G}}_{EP}(\mathbf{r}', \mathbf{r}) &= \hat{\mathbf{G}}_{EP}(\mathbf{r}, \mathbf{r}') \\ \hat{\mathbf{G}}_{HP}(\mathbf{r}', \mathbf{r}) &= -\hat{\mathbf{G}}_{EM}(\mathbf{r}, \mathbf{r}')\end{aligned}\tag{1.24}$$

In the main text, the diffraction efficiencies η_m can be obtained by transmitted power flow

going to the diffraction order represented by plane wave $\mathbf{E}_m, \mathbf{H}_m$:

$$\begin{aligned}\eta_m &= |t_m|^2 \\ &= \left| \int_{\Lambda} [\mathbf{E}(\mathbf{r}') \times \mathbf{H}_m^-(\mathbf{r}') - \mathbf{E}_m^-(\mathbf{r}') \times \mathbf{H}(\mathbf{r}')] \cdot \mathbf{n}_z d\mathbf{x} \right|^2\end{aligned}\quad (1.25)$$

where both fields are evaluated at the $\mathbf{r}' = (x, z_h)$ on the plane above the grating and the overlap integral is performed for a single grating period. For the sake of simplicity, we assume the permittivity distribution does not depend on y-axis. where both fields are evaluated at the $z = z_0$ plane above the grating, and the overlap integral is performed for a single grating period. The k -vector of $\mathbf{E}_m, \mathbf{H}_m$ is $(-k_x, 0, k_z)$ and k -vector of $\mathbf{E}_m^-, \mathbf{H}_m^-$ is $(k_x, 0, -k_z)$ and transmitted amplitude t_m is normalized by $|(\mathbf{E}_m \times \mathbf{H}_m^- - \mathbf{E}_m^- \times \mathbf{H}_m) \cdot \mathbf{n}_z| = 1$, where \mathbf{n}_z is unit vector along z -axis. Similar to Eq. 1.20 and 1.21, the change of η_m for a small perturbation in permittivity $\Delta\epsilon$ at a location \mathbf{r} in the grating layer is given by:

$$\begin{aligned}\Delta\eta_m &= 2\Re \left\{ t_m^* \int [\Delta\mathbf{E}(\mathbf{r}') \times \mathbf{H}_m^-(\mathbf{r}') \right. \\ &\quad \left. - \mathbf{E}_m^-(\mathbf{r}') \times \Delta\mathbf{H}(\mathbf{r}')] \cdot \mathbf{n}_z d\mathbf{x} \right\}\end{aligned}\quad (1.26)$$

Using Eq. 1.22 and 1.23, the derivative of diffraction efficiency with respect to permittivity is

$$\begin{aligned}\frac{\partial\eta_m}{\partial\epsilon(\mathbf{r})} &= 2\Re \left\{ t_m^* \int [\hat{\mathbf{G}}_{EP}(\mathbf{r}', \mathbf{r}) \mathbf{E}(\mathbf{r}) \times \mathbf{H}_m^-(\mathbf{r}') \right. \\ &\quad \left. - \mathbf{E}_m^-(\mathbf{r}') \times \hat{\mathbf{G}}_{HP}(\mathbf{r}', \mathbf{r}) \mathbf{E}(\mathbf{r})] \cdot \mathbf{n}_z d\mathbf{x} \right\}\end{aligned}\quad (1.27)$$

Applying the triple product rule of vector identities and reciprocity of Green's tensor in Eq.1.24, we obtain the adjoint field:

$$\begin{aligned}\frac{\partial\eta_m}{\partial\epsilon(\mathbf{r})} &= 2\Re \left(t_m^* \int \{ \hat{\mathbf{G}}_{EP}(\mathbf{r}, \mathbf{r}') [\mathbf{H}_m^-(\mathbf{r}') \times \mathbf{n}_z] \right. \\ &\quad \left. - \hat{\mathbf{G}}_{EM}(\mathbf{r}, \mathbf{r}') [\mathbf{E}_m^-(\mathbf{r}') \times \mathbf{n}_z] \} d\mathbf{x} \cdot \mathbf{E}(\mathbf{r}) \right) \\ &= 2\Re [t_m^* \mathbf{E}_{adj}(\mathbf{r}) \cdot \mathbf{E}(\mathbf{r})]\end{aligned}\quad (1.28)$$

where adjoint field $\mathbf{E}_{adj}(\mathbf{r})$ can be obtained by an solution of Maxwell's equation with illumination condition which is a plane wave generated by the polarization $(\mathbf{H}_m^-(\mathbf{r}') \times \mathbf{n}_z)$ and magnetization densities $(\mathbf{E}_m^-(\mathbf{r}') \times \mathbf{n}_z)$ from dipole expression.

2 Optimization based on Perturbation Approach

In this chapter, we use parameter reconstruction using the gradient of the figure of merit calculated by step-transition perturbation approach(STPA)

2.1 Process of optimization

Figure. shows an example of an one-dimensional binary phase grating profile characterized by depth, grating period, refractive indices, and transition points.

2.1.1 Figure of Merit

In this study, we use transition points as the set of design parameters $\mathbf{x} = [x_1 \cdots x_k \cdots x_{2K}]$ and define the figure of merit which depends on transition points position \mathbf{x} :

$$F(\mathbf{x}) = \sum_{m=-M}^M (\eta_m(\mathbf{x}) - \hat{\eta})^2 \quad (2.1)$$

where figure of merit $F(\mathbf{x})$ that represents the difference between the calculated diffraction efficiency $\eta_m(\mathbf{x})$ in orders and the average diffraction efficiency $\hat{\eta}$.

2.1.2 Design parameters

2.1.3 Initial design

2.1.4 Gradient calculation

The gradient of figure of merit with respect to the transition points $\nabla_{\mathbf{x}} F$ is crucial in determining the search direction to optima, which is the set of derivatives of figure of merit with respect

to each transition point, i.e.

$$\nabla_{\mathbf{x}} F = \left[\frac{\partial F}{\partial x_1}, \dots, \frac{\partial F}{\partial x_k}, \dots, \frac{\partial F}{\partial x_{2K}} \right] \quad (2.2)$$

To find these derivatives, we apply chain rule when differentiating $F(\mathbf{x})$.

$$\frac{\partial F}{\partial x_k} = \sum_{m=-N}^N \frac{\partial F}{\partial \eta_m} \cdot \frac{\partial \eta_m}{\partial x_k} \quad (2.3)$$

where the first term $\frac{\partial F}{\partial \eta_m}$ is easily calculated by using Eq. 2.1. The second term in Eq. 2.3, however, remains to be found. RCWA is used to calculate the diffraction efficiencies, $2K + 1$ system analyses are required to compute the gradient $\nabla_{\mathbf{x}} F$ because RCWA does not provide the analytical solution of derivatives of diffraction efficiency with respect to transition points $\frac{\partial \eta_m}{\partial x_k}$. Whereas, using STPA, we can describe an analytical solution of diffraction efficiency with respect to transition point positions of optical elements. It is allowed to calculate the gradient straightforwardly with accuracy as much as the approach based on the rigorous method if most of the features of the structure are bigger than the wavelength of the incident light.

2.2 One-dimensional diffractive optical elements

To apply the optimization method, we prepared several one-dimensional fan-out gratings which have different initial transition points position. The optimization result of a sample among them is introduced in this section. The one-dimensional fan-out grating with binary surface profiles has a $692nm$ height, 66 transition points, and $200\mu m$ grating period. The target image is a 117 spot array with equal spot intensity and spacing, and the full diffraction angle is 22° from -58^{th} to the 58^{th} diffraction orders. The refractive index of a dielectric layer is 1.46 for Fused silica, and that of the air layer is 1.00 were used.

2.2.1 Reconstruction results

Figure shows the diffraction properties of profile before and after optimization. To assess the uniformity in orders, we represent the value in orders as the difference of single diffraction efficiency of each order and the average one. Afterwhich, we compare the optimized results by gradient based on STPA and scalar TEA. We can observe that most of the values from optimized results with STPA are smaller compared to the initial results in Fig. Whereas, in the optimized results with TEA, there are no significant improvements over the initial results. For an accurate comparison, we calculated the total diffraction efficiency, UE in off-axis, and RMSE of 3 different profiles: Initial, STPA-based optimized, and TEA-based optimized one. These values are represented in Table. The optimized profile with STPA and TEA have scarcely less total efficiency than that of initial profile. Through STPA-based optimization there is considerable improvement in UE in off-axis from 26.47% to 12.39% and RMSE from 0.079% to 0.033%, while the improvement is small when using TEA-based optimization in UE in off-axis

from 26.47% to 22.72% and RMSE from 0.079% to 0.059%.

2.2.2 Experimental results

For the experimental verification, we used 641 *nm* wavelength laser source with TE-polarization and measured the sample 6 times with the same conditions. The average and standard deviation of measured diffraction efficiency in orders of the optimized sample are shown in the orange dot and error bar in Fig. To exclude the effects which may occur during measurement such as Fresnel reflection loss and power detector offset, both calculated and measured total diffraction efficiency were normalized to an identical value. Through the experimental results, we observed that the fabricated sample has UE in off-axis of 21.70% and RMSE of 0.061%. The values are different from the values obtained by calculation. The reason is that the diffraction efficiency in orders often strongly depends on the errors in fabrication processes, e.g., etching depth, feature width, slope steepness, features rounding. To investigate the effect of such fabrication errors, we simulated the effect of an under-etch or over-etch in the features of our optimized grating. The calculated results from the modified grating with 200 *nm* feature width deviation which including fabrication error are given in blue bar in the top of Fig. The simulated grating has UE in off-axis of 21.44% and RMSE of 0.064%. We observe positive agreement of the simulated data and the experimental data in the bottom of Fig. The average variation between the two data is 3.2% difference in diffraction efficiency in orders.

Based on the investigation, we would be able to overcome the performance degradation due to fabrication mismatch which is shown in the sample used for this works, because the problem is not about the limit of our fabrication facilities, e.g., the minimum feature size that a lithography system can print.

2.3 Limits of optimization by STPA

3 Optimization based on Adjoint-State Method

In this chapter we will see some examples of tables and figures.

3.1 Process of optimization

3.1.1 Binarization

In this section, we discuss our method for driving the dielectric continuum to discrete values of dielectric material and air and maintaining the fabricable minimum feature size over the iterative process. For the optimization, the starting point is a structure designed IFTA with applying a spatial filter to generate the dielectric continuum. We update a design density ρ which have a value from 0 to 1, rather than updating the permittivity distribution ϵ directly. For generating a structure with larger feature sizes, a spatial loss-pass filter can be applied to ρ to created a filtered density $\tilde{\rho}$:

$$\tilde{\rho}_i = \frac{\sum_{j \in \mathbb{N}_i} W_{ij} \rho_j}{\sum_{j \in \mathbb{N}_i} W_{ij}} \quad (3.1)$$

where \mathbb{N}_i denotes the design region, and W_{ij} is the weighting matrix, defined for a blurring radius of R as

$$W_{ij} = R - |r_i - r_j| \quad (3.2)$$

with $|r_i - r_j|$ being the distance between pixel i and j . This defines a spatial filter on ρ with the effect of smoothing out features with a length scale below R . The effect of this filter with 300 nm radius of R on a sample design density distribution is illustrated in Figure. The filtered geometry becomes then a binary pattern using projection function. We define $\bar{\rho}$ as the projected density, which is created from blurred density $\tilde{\rho}$ as

$$\bar{\rho}_i = \frac{\tanh(\beta t) + \tanh(\beta [\tilde{\rho}_i - t])}{\tanh(\beta t) + \tanh(\beta [1 - t])} \quad (3.3)$$

where t is a threshold factor between 0 and 1 which controls the threshold of the projection, typically 0.5, and β controls the strength of the projection, bigger value delivers harder binarization. The projected density distribution in Fig is recreated from blurred pattern in Fig. with $t = 0.5$ and $\beta = 300$. we also observe that the combination of circular spatial blurring filter and projection function can remove tiny features. The final relative permittivity distribution from the projected pattern is shown in Fig In addition, we can describe an analytical solution of the determination of $\frac{\partial \epsilon}{\partial \tilde{\rho}}$, $\frac{\partial \tilde{\rho}}{\partial \rho}$, $\frac{\partial \tilde{\rho}}{\partial \rho}$?, these filters can be combined with the derivatives of figure of merit calculated by adjoint method. The optimization problem is solved by limited-memory Broyden-Fletcher-Goldfarb-Shanno(L-BFGS) with bound constraints.

3.1.2 Critical demension

3.2 One-dimensional diffractive optical elements

3.2.1 Reconstruction results

3.2.2 Comparison with results by STPA

3.3 Two-dimensional diffractive optical elements

Two kinds of 2D fan-out gratings were selected for verification of the proposed design approach. First one is a common multi-spot generator which creates a 7×7 array of spots with equal intensity distribution, and the other generates a two-dimensional array of spots with the multilevel intensity distribution. To evaluate DOEs with various diffraction efficiency distribution, we define uniformity error (UE) and normalized root-mean-square error (NRMS) σ as follows:

$$UE = \frac{\tilde{\eta}_{\max} - \tilde{\eta}_{\min}}{\tilde{\eta}_{\max} + \tilde{\eta}_{\min}} \quad (3.4)$$

$$\sigma = \sqrt{\frac{1}{MN} \sum (\tilde{\eta}_{m,n} - \tilde{\eta}_{\text{obj}})^2} \quad (3.5)$$

where $\tilde{\eta}_{\max}$ and $\tilde{\eta}_{\min}$ represent the maximal and minimum intensity of the relative diffraction efficiency $\tilde{\eta} = \frac{\eta}{\eta_{\text{obj}}}$, respectively. The $\eta_{m,n}$ is the diffraction efficiency in orders on 2D array and M, N is the total number of diffraction orders along horizontal and vertical axis, respectively. The target diffraction efficiency distributions $\eta_{\text{obj}} \in [0, 1]^{m \times n}$ have uniform or specific entries. The spot energy distribution can be designed for any distribution meeting the application's requirements. The NRMS with scaled diffraction efficiency $\tilde{\eta}$ is preferable to with normal diffraction efficiency η because normalizing root-mean square error facilitates the comparison among various diffraction efficiency distributions with different scales from diverse DOEs. Lower values of both UE and NRMS indicate less residual variance so that our objective is to minimize UE and NRMS of a DOE design given certain diffraction efficiency distribution. The

fused silica (SiO_2) was selected as material for DOE. The refractive index of SiO_2 is assumed as $n_2 = 1.45$. transverse electric (TE)-polarized (i.e., E-field component along the y-axis) monochromatic light with a wavelength of $\lambda = 940\text{ nm}$ is incident wave from the substrate side with normal incidence angle. The grating period is $5\text{ }\mu\text{m} \times 5\text{ }\mu\text{m}$ and the pixel size is $100\text{ nm} \times 100\text{ nm}$. The depth of the grating was selected as $d = 1.18\text{ }\mu\text{m}$. Thus, the maximal diffraction angle of 7×7 and 7×5 diffractive beam splitter are about 53° at $(3,3)^{\text{th}}$ order and 43° at $(2,3)^{\text{th}}$ order from $(0,0)^{\text{th}}$ order, respectively.

3.3.1 Reconstruction results

To optimization this 7×7 diffractive beam splitter, we define our figure of merit as Eq. 2.1 with the uniform intensity distribution of target efficiency η_{obj} and find the local optima using L-BFGS with the gradient calculated by the adjoint method. The objective of this design is to create the grating structure can accurately diffract the incident light into 49 in different directions with equal intensity distribution. Figure shows the merit function as a function of the optimization iterations of 7×7 and 7×5 diffractive beam splitters. To minimize the modifications of the adjoint sensitivity, the projection strength factor incrementally increases every 10 iterations for binarization. This function results in immediate effects in the figure of merit, which can be visualized as disconnections on the dash lines. The figure of merit converged well and the algorithm found the optimum point after 80 iterations in both cases. The simulated diffraction efficiency distributions of DOEs before and after optimization is shown in Fig. These results are calculated for normally incident TE polarized light, i.e. the electric field component along the y-axis. In the diffraction pattern, the maximal diffraction angle is about 53° at $(3,3)^{\text{th}}$ order spot from the center. For an accurate comparison, we calculated the total diffraction efficiency, UE, and NRMS of two different situations of two diffractive beam splitters: Initial and optimized. The total diffraction efficiency of 49 spots of initial and optimized 7×7 spot-array generators are 79.96 %, and 79.71 %, respectively. this optimized element thus has no degradation in total efficiency while there is considerable improvement in UE from 63.79% to 16.35% and NRMS from 32.62% to 7.74%, through adjoint-based optimization. Over optimization process, 7×5 spot-array generator also has significant improvement in UE from 81.1% to 6.98% and NRMS from 37.93% to 3.78%. Moreover, total diffraction efficiency of 35 spots created by this DOE slightly increase from 74.45% to 78.48%. The numerical accuracy of these theoretical values, calculated by RCWA solver, and has less than 0.2% error has benchmarked in next section.

Furthermore, we applied our optimization method to the diffractive beam splitter with multi-level intensity distribution corresponding to Fig. As listed in Table 3.1, we specify different 9 groups have spot array with a specific intensity ratio, where group A, B, C, D, E, B', C', D' and E' have 1.0, 1.5, 2.0, 2.5, 1.0, 1.5, 2.0, 2.5 and 1.0 of intensity ratio, respectively. To optimize this diffractive beam splitter, we also use the figure of merit function in Eq. 2.1 with target efficiency distribution of above entries (see Table 3.1). Over the course of multiple iterations, the dielectric continuum in the device converges to the dielectric constant of either silica or

Table 3.1 – The target efficiency depends on groups in beam splitter with multilevel intensity distribution

Groups	A	B B'	C C'	D D'	E E'
Efficiency ratio	1.0	1.5	2.0	2.5	1.0
Target efficiency (%)	1.63	2.45	3.27	4.08	1.63

air from initial dielectric distribution designed by IFTA. We finally obtain a diffraction pattern distribution of optimized design nearly identical to the target pattern. The optimization convergence and pattern distribution before and after optimization are shown in the supplement 1. Quantitatively, total efficiency of this DOE slightly increase from 75.20 % to 78.28 % and UE and NRMS consequently reach 8.45 % from 74.73 % and 4.14 % from 55.15 %.

These results prove that the optimization algorithm is suitable for designing wide-angle diffractive beam splitters with various shapes of spot array and intensity distributions. Based on optimized designs, we fabricated and characterized diffractive beam-splitters. The detail experimental results are presented in the following section.

3.3.2 Experimental results

The diffractive beam splitters were fabricated by lithography using electron-beam and dry etching to create a chromium etch mask, and then by reactive ion etching to obtain SiO₂ binary surface relief structures. The optical elements are optically characterized using a TE-polarized 940 nm wavelength beam as our input source. We detect the diffracted light beams using a mobile single-pixel detector with a high dynamic range. To focus of both the simulation and experiment to facilitate a quantitative comparison, we normalized the measured results using scaling factor γ :

$$\gamma = \frac{\sum \eta_{m,n}^E \cdot \eta_{m,n}^S}{\sum |\eta_{m,n}^E|^2} \quad (3.6)$$

where $\eta_{m,n}^E, \eta_{m,n}^S$ are experimental and simulated efficiency in $(m, n)^{\text{th}}$ diffraction orders, respectively. The comparison between theoretical and experimental diffraction efficiencies of 7×7 and 7×5 beam-splitter creating uniform intensity array are presented in Table 3.2. The experimental data show that the DOEs operates with high-performance of uniformity. The UE of 7×7 and 7×5 beam splitters are measure to 23.35% and 14.42%, respectively, which is close to the calculated values. In addition, excellent agreement in NRMS values of the DOEs are observed between the simulation and the measurement. Little discrepancies between the simulated and experimental efficiencies are due in part to minor geometric imperfections in the fabricated samples. For an accurate comparison between theoretical and measured results, we analyze correlation of these data using mean absolute percentage deviation (MAPE)

3.3. Two-dimensional diffractive optical elements

Table 3.2 – Comparison with the theoretical and experimental properties of the 7×7 and 7×5 beam splitters.

	7 × 7 beam splitter		7 × 5 beam splitter	
	Calculated	Measured	Calculated	Measured
Total efficiency(%)	79.71	75.35	78.48	73.86
Normalized efficiency(%)		79.01		78.14
UE(%)	16.35	23.35	06.98	14.42
NRMS(%)	07.74	12.76	03.78	10.50

as a ratio defined by the formula:

$$\text{MAPE} = \frac{1}{MN} \sum \left| \frac{\eta_{m,n}^S - \eta_{m,n}^E}{\eta_{m,n}^S} \right| \quad (3.7)$$

where $\eta_{m,n}^S, \eta_{m,n}^E$ are simulated and experimental efficiency in $(m, n)^{\text{th}}$ diffraction orders and M, N is the total number of diffraction orders in two dimensional array. The MAPE of 7×7 and 7×5 beam splitters are calculated to 7.24 % and 5.00 %, respectively, which represents measurements demonstrate excellent reproducibility of the simulated results in a quantitative manner.

we also measured the diffraction efficiency of multi-intensity level beam splitter fabricated based on optimized design. A scanning electron microscopy (SEM) image of the optical element is presented in Fig, and theoretical and experimental diffraction efficiencies of beam splitter with array groups and their objective efficiency are summarized in Fig. Tilted SEM images of the beam-splitter show vertical sidewalls, indicative of high-quality etching. The experimental plot show that these elements operate with excellent agreement with respect to the objective in the overall intensity distributions. For an accurate comparison, we present the total diffraction efficiency, UE, and RMSE of simulated and measured one in Table 3.3. The UE and NRMS of fabricated sample are measured to 14.54 % and 9.81 %, respectively.

Table 3.3 – Comparison with the simulated and experimental properties of the beam splitters with multilevel diffraction intensity distribution.

	Simulated	Measured
Total efficiency (%)	78.27	74.20
Normalized efficiency (%)		77.99
UE (%)	08.46	14.54
NRMS (%)	04.14	09.81

Moreover, the results of the comparison show that the experimental results have a strong correlation with the theoretical results, where the MAPE of this beam splitter is calculated to 5.99 %. The only noticeable deviation in the measurement is a small mismatch of diffraction efficiency in a few orders the emerge due to minor fabrication errors. In general the diffraction

efficiency in orders often strongly depends on the errors in fabrication processes, e.g., etching depth, feature width, slope steepness, and feature rounding. Nevertheless, the fabricated samples based on optimized design overall display experimental performances which are significantly higher than the theoretical performances of initial designs before optimization. In other words, our methodology can readily create robust high-performance, multifunctional optical elements with wide-angle spot array that show theoretical and experimental performances that far exceed the current state-of-the-art recently reported

4 Experimental Verification and Fabrication Errors

4.1 Fabrication process

4.1.1 Laser direct writing

4.1.2 E-beam lithography

4.2 Measurement set-up

4.2.1 Fresnel loss

4.3 Fabrication errors

4.3.1 Edge shift

4.3.2 Effects of fabrication errors

4.3.3 Robust design

5 Conclusion and Perspectives

A An appendix

Lorem ipsum dolor sit amet, consectetur adipiscing elit. Ut purus elit, vestibulum ut, placerat ac, adipiscing vitae, felis. Curabitur dictum gravida mauris. Nam arcu libero, nonummy eget, consectetur id, vulputate a, magna. Donec vehicula augue eu neque. Pellentesque habitant morbi tristique senectus et netus et malesuada fames ac turpis egestas. Mauris ut leo. Cras viverra metus rhoncus sem. Nulla et lectus vestibulum urna fringilla ultrices. Phasellus eu tellus sit amet tortor gravida placerat. Integer sapien est, iaculis in, pretium quis, viverra ac, nunc. Praesent eget sem vel leo ultrices bibendum. Aenean faucibus. Morbi dolor nulla, malesuada eu, pulvinar at, mollis ac, nulla. Curabitur auctor semper nulla. Donec varius orci eget risus. Duis nibh mi, congue eu, accumsan eleifend, sagittis quis, diam. Duis eget orci sit amet orci dignissim rutrum.

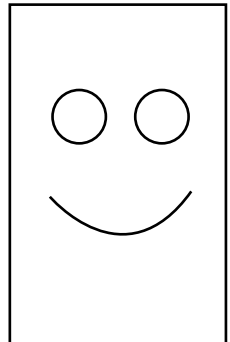


Personal details:

Name : Mr. Sample CV
Address : Samplestreet
70
6005 Luzern
Switzerland
Date of Birth : 2nd of October 1981
Nationality : Swiss
Legally work : legally work in EU
Marital status : with partner
Children : none

Languages : Chinese/Mandarin, English, French, German
Education level : Bachelors degree
Hospitality work experience : 3-5 years
Special experience : Europe work experience

Date of availability : September 2009
Current location : Africa
Travelling Status : will be travelling single status
Telephone : 0041 41 370 6759
Email address : jeff@h-g-r.com
Position(s) sought : Permanent position for graduates
Department(s) sought : Food & Beverage Bar/Sommelier



Personal profile:

As a Bachelor of Business Administration and after obtaining first relevant international work experience within the hospitality industry, I am now ready to take on new responsibilities to further my professional career. My key strengths include strong analytical and logical skills, an eye for detail, communication and interpersonal skills.
I enjoy working in a team and help others progress. At the same time I work well independently.
As a highly motivated and driven individual I strive on taking up challenges.

Interests:

Travelling
Foreign Cultures
Photography
Sports

Educational qualifications:

Oct 99 - Feb 02 Higher Diploma (Hotel Management)
Swiss Hotelmanagement School, SHL

Employment history:

Mar 04 - Ongoing	<p>Assistant Manager (Rooms Division/Food & Beverage)</p> <p>Hotel Atlantic Kempinski Hamburg www.kempinski.com 5 star business hotel, part of Leading Hotels of the World 412 guest rooms, large function facilities, 3 food & beverage outlets</p> <p>Optimization of bar procedures, reinforcing SOPs</p> <p>Developing & implementing promotions</p> <p>Responsible for day-to-day operations</p> <p>Optimization and streamlining of housekeeping and laundry procedures</p> <p>Implementation of new SOPs</p> <p>Analyzing monthly reports for rooms division performance and sub departments</p>
Mar 03 - Mar 04	<p>Management Trainee</p> <p>Hospitality Graduate Recruitment www.h-g-r.com Leading company for placements within the Hospitality industry.</p> <p>Traineeship covering all aspects of an online recruitment agency.</p>
Mar 02 - Mar 03	<p>Management Trainee (Rooms Division)</p> <p>Hyatt Regency Xian, China www.hyatt.com 5 star business hotel 404 guest rooms, 4 food & beverage outlets</p> <p>Traineeship covering all rooms division departments on operational as well as supervisory level.</p>

Training courses attended:

Mar 02 - Ongoing	OpenOffice - IT Courses
May 01 - Jan 03	Language Course - Chinese

References:

Hyatt Regency Xian
Patrick Sawiri, Phone: 86 22 2330 7654

Hospitality Graduate Recruitment
Jeff Ross, Phone: 41 41 370 99 88